ETH
Eidgenössische Technische Hochschule Zürich
Swiss Federal Institute of Technology Zurich

Implementation of impedance boundary conditions in HADAPT

Raffael Casagrande

Semester Thesis

Supervised by
Florian Krämer, Dr. Jörg Ostrowski
and Prof. Ralf Hiptmair

Zürich, July 2012

Abstract

Impedance boundary conditions (IBC) are added to a Robust Maxwell Formulation (Hiptmair et al. [2008]) and implemented in the three dimensional finite element code HADAPT. The IBC lead to a substantial decrease in the number of unknowns which allows for an efficient but approximative solution of boundary layer problems. The approximation error is determined and analyzed for simple test geometries.

Contents

1 Introduction **1**

2 Derivation of the variational equations **3**
2.1 Geometric description 3
2.2 Maxwell's equations for linear materials 4
2.3 $\mathbf{a} - \varphi$ formalism 5
2.4 Transformation to frequency domain 6
2.5 Variational formulation 7
2.6 Robust Maxwell Formulation 8
2.7 Impedance boundary conditions 12
2.8 Implemented variational equations 13

3 Implementation in HADAPT **14**
3.1 Assembling the matrices 14
3.2 Solving the equations 15

4 Numerical Experiments **16**
4.1 Description of test cases 16
4.2 Runtime and memory requirements 17
4.3 Comparison to Infolytica 18
4.4 Accuracy of the IBC 22

5 Conclusion **24**

1 Introduction

In the design of electric power devices one often has to account for currents which are induced by other, stronger electric currents. As an example consider the configuration given in Fig. 1.1: A semi-infinite conductor occupies the space $z > 0$. The region in which $z < 0$ is filled with air and a spatially constant magnetic field $h_x = h_0 \cos(\omega t)$ is present which induces a current in the conductor. Across the interface $z = 0$ the permittivity jumps from μ_0 to μ and the conductivity from 0 to σ.

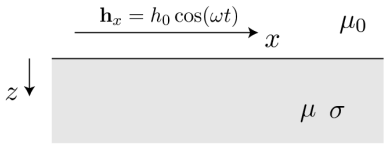

Figure 1.1: A spatially constant magnetic field h_x induces a current in the semi-infinite conductor ($z > 0$).

By assuming zero displacement current Jackson [Jackson, 1998][p. 221] derives an explicit formula for the y-component of the electric current (for $z > 0$):

$$j_y = \frac{\sqrt{2}}{\delta} H_0 e^{-z/\delta} \cos(z/\delta - \omega t + 3\pi/4) \tag{1.1}$$

where the *penetration depth* δ is given by

$$\delta = \sqrt{\frac{2}{\mu\omega\sigma}}.$$

Eq. (1.1) shows that the electric current is decaying exponentially towards the inside of the conductor and that the penetration depth decreases with increasing frequency ω. In other words a boundary layer is formed which becomes narrower as the frequency increases. In order to resolve this boundary layer with a traditional Finite Element Method (FEM) very high spatial resolution is required which in turn requires a lot of computing power.

Impedance boundary conditions (IBC) are often used as an approximation to overcome this deficiency. They essentially assume a field of the form given in Eq. (1.1) inside the conductor and resolve the electromagnetic fields only along the boundary. The aim

of this thesis was to implement IBC in HADAPT, a FEM suite developed by ABB Switzerland Ltd.. which uses the Robust Maxwell Formulation introduced in Hiptmair et al. [2008].

This document starts with a detailed derivation of the governing equations and a thorough discussion of IBC (Chap. 2). After a compact summary of implementation specific aspects (Chap. 3) a rich set of numerical results is presented and discussed (Chap. 4). Chap. 5 gives a short synopsis of the most important results.

2 Derivation of the variational equations

This chapter shows the derivation of the variational equations which are implemented in HADAPT. It starts from the general Maxwell's equations which are then reformulated in terms of $\mathbf{a} - \varphi$ and transformed to the frequency domain. In accordance with Hiptmair et al. [2008] an additional equation is added to stabilize Maxwell's equations for low frequencies and the variational formulation is derived. Finally the impedance boundary conditions (IBC) are incorporated.

2.1 Geometric description

An artificially bounded domain $\Omega \in \mathbb{R}^3$ which is composed of three distinct subdomains: $\Omega = \Omega_a \cup \Omega_i \cup \Omega_w$ is considered. Ω_i is the domain of the IBC conductor, Ω_w the domain of the (exciting) conductor/wire and Ω_a contains the air box around the conductors (see Fig. 2.1). Please note that the IBC conductor must be surrounded by the air box Ω_a. In order to simplify notation the computational domain $\Omega_c = \Omega_a \cup \Omega_w$ is defined.

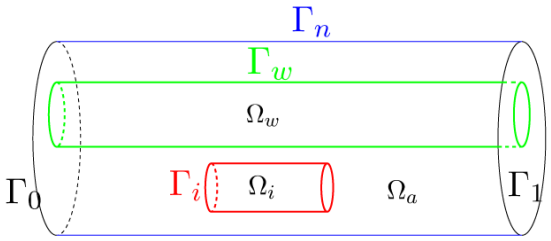

Figure 2.1: The geometric situation.

There are several boundaries for each type of boundary condition:

Γ_0	Left voltage boundary condition ($\varphi = 0$),
Γ_1	Right voltage boundary condition ($\varphi = U$),
Γ_n	Natural boundary condition,
Γ_w	Boundary of the (exciting) conductor,
Γ_i	Boundary of IBC conductor.

Please note that only Γ_w intersects with Γ_0 and Γ_1, all other boundaries do not intersect with each other.

2.2 Maxwell's equations for linear materials

According to [Nolting, 2007, p. 214] Maxwell's equations for an arbitrary material are given by

$$\operatorname{div} \mathbf{b} = 0 \tag{2.1a}$$

$$\mathbf{curl}\, \mathbf{e} + \frac{\partial \mathbf{b}}{\partial t} = 0 \tag{2.1b}$$

$$\operatorname{div} \mathbf{d} = \rho \tag{2.1c}$$

$$\mathbf{curl}\, \mathbf{h} - \frac{\partial \mathbf{d}}{\partial t} = \mathbf{j}. \tag{2.1d}$$

where $\mathbf{b}$ and $\mathbf{e}$ denote the magnetic and electric field, respectively. ρ stands for the charge density and $\mathbf{j}$ denotes the current density.

Remark. By taking the divergence of (2.1d) it is seen that the charges are preserved in the system:

$$\underbrace{\operatorname{div} \mathbf{curl}\, \mathbf{h}}_{=0} - \operatorname{div} \frac{\partial \mathbf{d}}{\partial t} = \operatorname{div} \mathbf{j} \tag{2.2}$$

$$\overset{(2.1c)}{\Leftrightarrow} \qquad \frac{\partial \rho}{\partial t} + \operatorname{div} \mathbf{j} = 0. \tag{2.3}$$

Assumption. Only linear materials are considered. The constitutive relations are

$$\begin{aligned} \mathbf{b} &= \mu_r \mu_0 \mathbf{h} &&= \mu \mathbf{h} \\ \mathbf{d} &= \varepsilon_r \varepsilon_0 \mathbf{e} &&= \varepsilon \mathbf{e}, \end{aligned} \tag{2.4}$$

where μ is the permeability and ε the electric permittivity of the material.

Assumption. The current $\mathbf{j}$ can be expressed with Ohm's Law:

$$\mathbf{j} = \sigma \mathbf{e}, \tag{2.5}$$

where σ denotes the electric conductivity.

Therefore Maxwell's equations for linear materials are given by

$$\operatorname{div} \mathbf{b} = 0 \tag{2.6a}$$

$$\mathbf{curl}\, \mathbf{e} + \frac{\partial \mathbf{b}}{\partial t} = 0 \tag{2.6b}$$

$$\operatorname{div} \varepsilon \mathbf{e} = \rho \tag{2.6c}$$

$$\mathbf{curl}\, \frac{1}{\mu} \mathbf{b} - \frac{\partial \varepsilon \mathbf{e}}{\partial t} = \mathbf{j}. \tag{2.6d}$$

2.3 $\mathbf{a} - \varphi$ formalism

The four Eqs. (2.6) can be reduced to two equations by introducing the scalar potential φ and the vector potential $\mathbf{a}$ such that

$$\mathbf{b} = \mathbf{curl}\,\mathbf{a}, \tag{2.7}$$

$$\mathbf{e} = -\,\mathbf{grad}\,\varphi - \frac{\partial \mathbf{a}}{\partial t}. \tag{2.8}$$

If the above equations are inserted in Eqs. (2.6) the homogeneous equations (2.6a) and (2.6b) are automatically fulfilled. The remaining inhomogeneous equations (2.6c) and (2.6d) become

$$-\operatorname{div}\varepsilon\,\mathbf{grad}\,\varphi - \frac{\partial}{\partial t}\operatorname{div}\varepsilon\mathbf{a} = \rho \tag{2.9a}$$

$$\mathbf{curl}\,\frac{1}{\mu}\,\mathbf{curl}\,\mathbf{a} + \varepsilon\,\mathbf{grad}\,\frac{\partial\varphi}{\partial t} + \varepsilon\frac{\partial^2\mathbf{a}}{\partial t^2} = \mathbf{j}. \tag{2.9b}$$

With this trick it was possible to reduce a system of four first order partial differential equations to a pair of second order partial differential equations which are generally easier to solve on the computer.

Remark. Eqs. (2.9) define $\mathbf{a}$ and φ not uniquely. This becomes clear by adding a rotation free component, $\mathbf{grad}\,\chi$, to $\mathbf{a}$ and φ:

$$\mathbf{a}' = \mathbf{a} + \mathbf{grad}\,\chi \tag{2.10}$$

$$\varphi' = \varphi - \frac{\partial\chi}{\partial t}. \tag{2.11}$$

The last term in Eq. (2.11) was chosen such that the electric field derived from φ and φ' is the same, i.e. $\mathbf{e} = -\,\mathbf{grad}\,\varphi - \frac{\partial\mathbf{a}}{\partial t} = -\,\mathbf{grad}\,\varphi' - \frac{\partial\mathbf{a}'}{\partial t}$. Clearly the same holds for the magnetic field: $\mathbf{b} = \mathbf{curl}\,\mathbf{a} = \mathbf{curl}\,\mathbf{a}'$ and therefore $\mathbf{a}'$ and φ' fulfill Eqs. (2.9) as well.

In order to assure that Eqs. (2.9) have a unique solution the Coulomb gauge condition,

$$\operatorname{div}\varepsilon\mathbf{a} = 0, \tag{2.12}$$

is added. If $\mathbf{a}$ fulfills Eq. (2.12) and a magnetic field $\mathbf{b}$ is given, $\mathbf{a}$ is well-defined up to a constant. This can be shown by using the Helmholtz decomposition of $\mathbf{a}$ [Nolting, 2007, p.36].

In conclusion Maxwell's equations (2.6) can be expressed equivalently in the $\mathbf{a} - \varphi$ formalism as

$$-\operatorname{div}\varepsilon\,\mathbf{grad}\,\varphi = \rho \tag{2.13a}$$

$$\mathbf{curl}\,\frac{1}{\mu}\,\mathbf{curl}\,\mathbf{a} + \varepsilon\,\mathbf{grad}\,\frac{\partial\varphi}{\partial t} + \varepsilon\frac{\partial^2\mathbf{a}}{\partial t^2} = \mathbf{j} \tag{2.13b}$$

$$\operatorname{div}\varepsilon\mathbf{a} = 0. \tag{2.13c}$$

It can be shown that this system of partial differential equations equipped with appropriate boundary conditions defines φ and $\mathbf{a}$ uniquely.

2.4 Transformation to frequency domain

Assumption. The electric- and magnetic field are oscillating at the frequency $\omega \in \mathbb{R}$.

This assumption is often justified if the boundary conditions are oscillating at the same frequency ω and after the system has passed an transient calibration phase. Therefore the electric and magnetic fields can be split in a spatial and a transient part:

$$\mathbf{e}(\mathbf{x}, t) = \mathrm{Re}\left[\hat{\mathbf{e}}(\mathbf{x}) \cdot \exp(i\omega t)\right] \tag{2.14}$$

$$\mathbf{b}(\mathbf{x}, t) = \mathrm{Re}\left[\hat{\mathbf{b}}(\mathbf{x}) \cdot \exp(i\omega t)\right]. \tag{2.15}$$

By inserting Eq. (2.14) in Ohm's Law (2.5) it is seen that the the current density $\mathbf{j}$ is also oscillating at frequency ω. By using the continuity equation (2.3) one can further show that ρ is composed of a transient, oscillating part and a spatial part, that is:

$$\rho(\mathbf{x}, t) = \mathrm{Re}\left[\hat{\rho}(\mathbf{x}) \cdot \exp(i\omega t)\right] \tag{2.16}$$

$$\mathbf{j}(\mathbf{x}, t) = \mathrm{Re}\left[\hat{\mathbf{j}}(\mathbf{x}) \cdot \exp(i\omega t)\right]. \tag{2.17}$$

Eqs. (2.14) and (2.15) imply that the $\mathbf{a}$ and φ fields are also split in a transient and a spatial part:

$$\mathbf{a}(\mathbf{x}, t) = \mathrm{Re}\left[\hat{\mathbf{a}}(\mathbf{x}) \cdot \exp(i\omega t)\right] \tag{2.18}$$

$$\varphi(\mathbf{x}, t) = \mathrm{Re}\left[\hat{\varphi}(\mathbf{x}) \cdot \exp(i\omega t)\right]. \tag{2.19}$$

In order to formulate Maxwell's Equations in the frequency domain the above equations are inserted in the system of equations (2.13):

$$-\operatorname{div} \varepsilon \, \mathbf{grad}\, \hat{\varphi} = \hat{\rho} \tag{2.20a}$$

$$\mathbf{curl}\, \frac{1}{\mu}\, \mathbf{curl}\, \hat{\mathbf{a}} + i\varepsilon\omega\, \mathbf{grad}\, \hat{\varphi} - \varepsilon\omega^2 \hat{\mathbf{a}} = \hat{\mathbf{j}} \tag{2.20b}$$

$$\operatorname{div} \varepsilon \hat{\mathbf{a}} = 0. \tag{2.20c}$$

This system of partial differential equations contains only the complex, spatial functions $\hat{\varphi}$, $\hat{\mathbf{a}}$, $\hat{\mathbf{j}}$ and $\hat{\rho}$. Once this system, equipped with the appropriate boundary conditions, is solved the quantities of interest can be calculated with Eqs. (2.14) - (2.19).

Remark. Maxwell's equations in the frequency domain can also be interpreted using Fourier theory, i.e. the potential φ can be written as:

$$\varphi(\mathbf{x}, t) = \int_{-\infty}^{\infty} \hat{\varphi}(\mathbf{x}, \omega) \cdot \exp(i\omega t)\, \mathrm{d}\omega.$$

A similar idea is used for the remaining unknowns, $\mathbf{a}$, $\mathbf{j}$ and ρ. If this ansatz is then inserted into the transient Maxwell's equations (2.13) one sees that Maxwell's equations in the frequency domain (2.20) have to hold for all frequencies ω.

Ohm's Law (2.5) and the continuity equation (2.3) in the frequency domain are given by

$$\hat{\mathbf{j}} = \sigma\hat{\mathbf{e}} = -\sigma\,\mathbf{grad}\,\hat{\varphi} - i\sigma\omega\mathbf{a} \tag{2.21}$$

$$i\omega\hat{\rho} + \operatorname{div}\hat{\mathbf{j}} = 0. \tag{2.22}$$

The last equation provides a relation between the current density $\hat{\mathbf{j}}$ and the charge density $\hat{\rho}$ if $\omega > 0$. We can thus insert (2.21) and (2.22) into the system (2.20):

$$i\omega \operatorname{div}\varepsilon\,\mathbf{grad}\,\hat{\varphi} = -\operatorname{div}\left[\sigma\,\mathbf{grad}\,\hat{\varphi} + i\sigma\omega\hat{\mathbf{a}}\right] \tag{2.23a}$$

$$\mathbf{curl}\,\frac{1}{\mu}\,\mathbf{curl}\,\hat{\mathbf{a}} + i\varepsilon\omega\,\mathbf{grad}\,\hat{\varphi} - \varepsilon\omega^2\hat{\mathbf{a}} = -\left[\sigma\,\mathbf{grad}\,\hat{\varphi} + i\sigma\omega\hat{\mathbf{a}}\right] \tag{2.23b}$$

$$\operatorname{div}\varepsilon\hat{\mathbf{a}} = 0. \tag{2.23c}$$

By taking divergence of Eq. (2.23b),

$$\underbrace{\operatorname{div}\mathbf{curl}\,\frac{1}{\mu}\,\mathbf{curl}\,\hat{\mathbf{a}}}_{=0} + i\omega \operatorname{div}\varepsilon\,\mathbf{grad}\,\hat{\varphi} - \omega^2\underbrace{\operatorname{div}\varepsilon\hat{\mathbf{a}}}_{\overset{(2.23c)}{=}0} = -\operatorname{div}\left[\sigma\,\mathbf{grad}\,\hat{\varphi} + i\sigma\omega\hat{\mathbf{a}}\right], \tag{2.24}$$

it is seen that the Gauss Law (2.23a) is contained in (2.23b) and (2.23c) for $\omega > 0$. Therefore Eq. (2.23a) is redundant and Maxwell's equations can be written as

$$\mathbf{curl}\,\frac{1}{\mu}\,\mathbf{curl}\,\hat{\mathbf{a}} + i\varepsilon\omega\,\mathbf{grad}\,\hat{\varphi} - \varepsilon\omega^2\hat{\mathbf{a}} = -\left[\sigma\,\mathbf{grad}\,\hat{\varphi} + i\sigma\omega\hat{\mathbf{a}}\right] \tag{2.25a}$$

$$\operatorname{div}\varepsilon\hat{\mathbf{a}} = 0. \tag{2.25b}$$

Remark. In order to simplify notation the hat ˆ is left out in the upcoming sections. Until now it has been used to denote variables in the frequency domain, but from now on all variables are assumed to lie in the frequency domain unless explicitly noted.

2.5 Variational formulation

The variational equations of the strong formulation (2.25) rely on the Sobolev spaces (see [Hiptmair et al., 2008])

$$V := \left\{\mathbf{v} \in \boldsymbol{H}(\mathbf{curl}, \Omega_c) : \mathbf{curl}_\Gamma\,\mathbf{v}_t = 0 \text{ on } \partial\Omega_c, \int_\tau \mathbf{v}\cdot\underline{\mathrm{d}}s = 0\right\} \tag{2.26}$$

$$H(U) := \left\{\psi \in H^1(\Omega_c) : \psi_{|\Gamma_0} = 0, \psi_{\Gamma_1} = U\right\} \tag{2.27}$$

We assume the strong form (2.20) holds in the computational domain Ω_c and test it with test functions $\mathbf{a}' \in V$, $\varphi' \in H(0)$:

$$\int_{\Omega_c} \mathbf{curl}\, \frac{1}{\mu}\, \mathbf{curl}\, \mathbf{a} \cdot \mathbf{a}' + (i\omega\varepsilon + \sigma)\, \mathbf{grad}\, \varphi \cdot \mathbf{a}' - (\omega^2\varepsilon - i\sigma\omega)\mathbf{a} \cdot \mathbf{a}' \,\mathrm{d}\mathbf{x} = 0 \tag{2.28a}$$

$$\int_{\Omega_c} \operatorname{div} \varepsilon\mathbf{a} \cdot \varphi' \,\mathrm{d}\mathbf{x} = 0. \tag{2.28b}$$

Stokes's formula.

$$\int_{\Omega} \mathbf{curl}\, \mathbf{v} \cdot \mathbf{u} - \mathbf{curl}\, \mathbf{u} \cdot \mathbf{v} \,\mathrm{d}\mathbf{x} = \int_{\partial\Omega} (\mathbf{u} \times \mathbf{n}) \cdot \mathbf{v} \,\mathrm{d}S \qquad \forall \mathbf{u} \in \boldsymbol{H}(\mathbf{curl}, \Omega),\, \mathbf{v} \in \boldsymbol{H}^1(\Omega) \tag{2.29}$$

Green's first formula. *For all vector fields* $\mathbf{j} \in \left(C^1_{pw}(\Omega)\right)^d$ *and functions* $v \in C^1_{pw}(\Omega)$ *holds*

$$\int_{\Omega} \mathbf{j} \cdot\ \boldsymbol{grad}\, v \,\mathrm{d}\mathbf{x} = -\int_{\Omega} \operatorname{div} \mathbf{j}\, v \,\mathrm{d}\mathbf{x} + \int_{\partial\Omega} \mathbf{j} \cdot \mathbf{n}\, v \,\mathrm{d}S \tag{2.30}$$

With the help of Stokes's formula the first terms of Eq. (2.28a) can be rewritten as follows:

$$\int_{\Omega_c} \mathbf{curl}\, \frac{1}{\mu}\, \mathbf{curl}\, \mathbf{a} \cdot \mathbf{a}' \,\mathrm{d}\mathbf{x} = \int_{\Omega_c} \frac{1}{\mu}\, \mathbf{curl}\, \mathbf{a} \cdot \mathbf{curl}\, \mathbf{a}' \mathrm{d}\mathbf{x} - \int_{\partial\Omega_c} \frac{1}{\mu}\, (\mathbf{curl}\, \mathbf{a} \times \mathbf{n}) \cdot \mathbf{a}' \,\mathrm{d}S \tag{2.31}$$

By using Green's first formula the derivative in Eq. (2.28b) is shifted onto φ' and the weak formulation is obtained: Find $\mathbf{a} \in V, \varphi \in H(U)$ such that:

$$\left(\frac{1}{\mu}\, \mathbf{curl}\, \mathbf{a}, \mathbf{curl}\, \mathbf{a}'\right)_{\Omega_c} + \left((i\omega\varepsilon + \sigma)\, \mathbf{grad}\, \varphi, \mathbf{a}'\right)_{\Omega_c} - \left((\omega^2\varepsilon - i\omega\sigma)\mathbf{a}, \mathbf{a}'\right)_{\Omega_c} - \int_{\partial\Omega_c} \frac{1}{\mu}\, (\mathbf{curl}\, \mathbf{a} \times \mathbf{n}) \cdot \mathbf{a}' \,\mathrm{d}S = 0 \tag{2.32a}$$

$$-\left(\varepsilon\mathbf{a},\, \mathbf{grad}\, \varphi'\right)_{\Omega_c} + \int_{\partial\Omega_c} \varepsilon\mathbf{a} \cdot \mathbf{n}\, \varphi' \,\mathrm{d}S = 0 \tag{2.32b}$$

for all $\mathbf{a}' \in V, \varphi' \in H(0)$. $(u, v)_{\Omega} = \int_{\Omega} u \cdot v \,\mathrm{d}\mathbf{x}$ was used to denote the L^2 inner product.

2.6 Robust Maxwell Formulation

When the Eqs. (2.32) are solved numerically it is observed that the resulting linear system becomes ill-conditioned for $\omega \to 0$. In the limiting case $\omega = 0$ the equations of stationary electromagnetism have to hold. They can be derived from Maxwell's equations (2.13)

by setting time derivatives to zero:

$$-\operatorname{div}\varepsilon\,\mathbf{grad}\,\varphi = \rho \tag{2.33a}$$

$$\mathbf{curl}\,\frac{1}{\mu}\,\mathbf{curl}\,\mathbf{a} = -\sigma\,\mathbf{grad}\,\varphi \tag{2.33b}$$

$$\operatorname{div}\varepsilon\mathbf{a} = 0. \tag{2.33c}$$

In contrast Maxwell's equations in the frequency domain (2.25) become in the limit $\omega \to 0$:

$$\mathbf{curl}\,\frac{1}{\mu}\,\mathbf{curl}\,\mathbf{a} = -\sigma\,\mathbf{grad}\,\varphi \tag{2.34}$$

$$\operatorname{div}\varepsilon\mathbf{a} = 0. \tag{2.35}$$

By taking the divergence of Eq. (2.34) we get,

$$-\operatorname{div}\sigma\,\mathbf{grad}\,\varphi = 0. \tag{2.36}$$

Inside a idealized conductor without free charges ($\rho = 0$) in which σ, μ and ε are constant and greater than zero Eq. (2.36) is equivalent to the Gauss Law (2.33a). However outside the conductor the Gauss Law (2.33a) is missing which implies that Eqs. (2.25) become unstable for $\omega \to 0$.

Hiptmair et al. [2008] describe this phenomena in more detail and propose to stabilize the Eqs. (2.32) by splitting the scalar field φ in two components,

$$\varphi = \tilde{\varphi} + \psi, \tag{2.37}$$

where $\tilde{\varphi} \in H(U)$ and $\psi \in H^1_e(U)$ with

$$H^1_e(U) := \left\{ \begin{array}{l} v \in H^1(\Omega_c) : v \equiv \text{const} \\ \text{on all connected components of } \Omega_w, \\ v_{|\Gamma_0} = 0, v_{|\Gamma_1} = 0, v_{|\Gamma_i} = \text{const.} \end{array} \right\}. \tag{2.38}$$

The introduction of an extra unknown must be balanced by an extra equation. This can be accomplished in two ways:

Option 1: By testing (2.25a) with $\mathbf{grad}\,\psi$: The resulting weak formulation is simply obtained by inserting $\mathbf{a}' = \mathbf{grad}\,\psi$ in (2.32a):

$$-\int_{\partial\Omega_c} \frac{1}{\mu}\,(\mathbf{curl}\,\mathbf{a} \times \mathbf{n}) \cdot \mathbf{grad}\,\psi'\,\mathrm{d}S + \left((i\omega\varepsilon + \sigma)\,\mathbf{grad}\,\varphi,\, \mathbf{grad}\,\psi'\right)_{\Omega_c} - \left((\omega^2\varepsilon - i\omega\sigma)\mathbf{a},\, \mathbf{grad}\,\psi'\right)_{\Omega_c} = 0 \tag{2.39}$$

because $\mathbf{grad}\,\psi' = 0$ inside Ω_w, $(\sigma\,\chi,\, \mathbf{grad}\,\psi') = 0$ for any χ. With the help of the gauge condition (2.32b), (2.39) can thus be rewritten as

$$-\int_{\partial\Omega_c} \frac{1}{\mu}\,(\mathbf{curl}\,\mathbf{a}\times\mathbf{n})\cdot\,\mathbf{grad}\,\psi'\,\mathrm{d}S + (i\omega\varepsilon\,\mathbf{grad}\,(\tilde{\varphi}+\psi),\,\mathbf{grad}\,\psi')_{\Omega_c} - \omega^2\int_{\partial\Omega_c}\varepsilon\mathbf{a}\cdot\mathbf{n}\psi'\,\mathrm{d}S = 0 \quad (2.40)$$

Option 2: The supplementary equation is derived by testing the missing Gauss law (2.23a) with ψ':

$$\int_{\Omega_c} i\omega\,\mathrm{div}\,[\varepsilon\,\mathbf{grad}\,\varphi]\;\psi'\,\mathrm{d}\mathbf{x} + \int_{\Omega_c}\mathrm{div}\,[\sigma\,\mathbf{grad}\,\varphi + i\omega\sigma\mathbf{a}]\psi'\,\mathrm{d}\mathbf{x} = 0 \quad (2.41)$$

$$\Leftrightarrow \quad -i\omega\int_{\Omega_c}\varepsilon\,\mathbf{grad}\,\varphi\cdot\,\mathbf{grad}\,\psi'\,\mathrm{d}\mathbf{x} + i\omega\int_{\partial\Omega_c}\varepsilon\psi'\,\mathbf{grad}\,\varphi\cdot\mathbf{n}\,\mathrm{d}S - \underbrace{\int_{\Omega_c}\sigma(\,\mathbf{grad}\,\varphi + i\omega\mathbf{a})\,\mathbf{grad}\,\psi'\,\mathrm{d}\mathbf{x}}_{=0} + \underbrace{\int_{\partial\Omega_c}\sigma((\,\mathbf{grad}\,\varphi + i\omega\mathbf{a})\cdot\mathbf{n}\psi'\,\mathrm{d}S}_{=0} = 0 \quad (2.42)$$

where the last term is zero because $\psi' = 0$ on Γ_0 and Γ_1 and $\sigma = 0$ on the remaining boundary. Thus an alternative form of (2.40) is obtained:

$$-(\varepsilon\,\mathbf{grad}\,(\tilde{\varphi}+\psi),\,\mathbf{grad}\,\psi')_{\Omega_a} + \int_{\partial\Omega_c}\varepsilon\psi'\,\mathbf{grad}\,\varphi\cdot\mathbf{n}\,\mathrm{d}S = 0, \quad (2.43)$$

which equals the Gauss law in the non-conducting domain.

Equivalence of form 1 and 2: One can show that the two forms (2.40) and (2.43) of the additional equation are equivalent:

$$\begin{aligned}
&\int_{\partial\Omega_c}\frac{1}{\mu}\,(\mathbf{curl}\,\mathbf{a}\times\mathbf{n})\cdot\,\mathbf{grad}\,\psi'\,\mathrm{d}S \\
&\qquad\overset{(2.31)}{=} 0 - \int_{\Omega_c}\mathbf{curl}\,\frac{1}{\mu}\,\mathbf{curl}\,\mathbf{a}\cdot\,\mathbf{grad}\,\psi'\mathrm{d}\mathbf{x} \\
&\qquad\overset{(2.30)}{=} 0 - \int_{\partial\Omega_c}\mathbf{curl}\,\frac{1}{\mu}\,\mathbf{curl}\,A\cdot\mathbf{n}\psi'\,\mathrm{d}S \\
&\qquad\overset{(2.25a)}{=} \int_{\partial\Omega_c}\Big(i\omega\varepsilon\,\mathbf{grad}\,\varphi - \omega^2\varepsilon\mathbf{a} + \sigma(\,\mathbf{grad}\,\varphi + i\omega\mathbf{a})\Big)\cdot\mathbf{n}\,\psi'\,\mathrm{d}S
\end{aligned}$$

Hence Eq. (2.40) can be rewritten as

$$-i\omega\int_{\partial\Omega_c}\varepsilon\,\mathbf{grad}\,\varphi\cdot\mathbf{n}\psi'\,\mathrm{d}S - \underbrace{\int_{\partial\Omega_c}\sigma(\,\mathbf{grad}\,\varphi + i\omega\mathbf{a})\cdot\mathbf{n}\,\psi'\,\mathrm{d}S}_{=0} + \omega^2\int_{\partial\Omega_c}\varepsilon\mathbf{a}\cdot\mathbf{n}\psi'\,\mathrm{d}S + i\omega\,(\varepsilon\,\mathbf{grad}\,(\tilde{\varphi}+\psi),\,\mathbf{grad}\,\psi')_{\Omega_c} - \omega^2\int_{\partial\Omega_c}\varepsilon\mathbf{a}\cdot\mathbf{n}\psi'\,\mathrm{d}S = 0, \quad (2.44)$$

which equals exactly the second formulation (2.43).

Summary: Robust Maxwell formulation In order to derive the Robust Maxwell formulation the splitting (2.37) is inserted into Eqs. (2.32) and the supplementary equations (2.40) and (2.43) are added: Find $\mathbf{a} \in V, \tilde{\varphi} \in H(U), \psi \in H_e^1(U)$ such that:

$$\boxed{\begin{aligned}
&\left(\frac{1}{\mu}\,\mathbf{curl}\,\mathbf{a}, \mathbf{curl}\,\mathbf{a}'\right)_{\Omega_c} - \int_{\partial\Omega_c} \frac{1}{\mu}\,(\mathbf{curl}\,\mathbf{a}\times\mathbf{n})\cdot\mathbf{a}'\,\mathrm{d}S - \\
&\left((\omega^2\varepsilon - i\omega\sigma)\mathbf{a}, \mathbf{a}'\right)_{\Omega_c} + \left((i\omega\varepsilon+\sigma)\,\mathbf{grad}\,\tilde{\varphi}, \mathbf{a}'\right)_{\Omega_c} + \left(i\omega\varepsilon\,\mathbf{grad}\,\psi, \mathbf{a}'\right)_{\Omega_c} = 0 && \text{(A)}\\
&-\left(\varepsilon\mathbf{a},\,\mathbf{grad}\,\tilde{\varphi}'\right)_{\Omega_c} + \int_{\partial\Omega_c} \varepsilon\mathbf{a}\cdot\mathbf{n}\,\tilde{\varphi}'\,\mathrm{d}S = 0 && \text{(B)}\\
&-\int_{\partial\Omega_c} \frac{1}{\mu}\,(\mathbf{curl}\,\mathbf{a}\times\mathbf{n})\cdot\,\mathbf{grad}\,\psi'\,\mathrm{d}S - \omega^2\int_{\partial\Omega_c}\varepsilon\mathbf{a}\cdot\mathbf{n}\psi'\,\mathrm{d}S + \\
&\qquad\left(i\omega\varepsilon\,\mathbf{grad}\,(\tilde{\varphi}+\psi),\,\mathbf{grad}\,\psi'\right)_{\Omega_a} = 0 && \text{(C)}\\
&-\left(\varepsilon\,\mathbf{grad}\,(\tilde{\varphi}+\psi),\,\mathbf{grad}\,\psi'\right)_{\Omega_a} + \int_{\partial\Omega_c}\varepsilon\psi'\,\mathbf{grad}\,\varphi\cdot\mathbf{n}\,\mathrm{d}S = 0 && \text{(C*)}
\end{aligned}}$$

for all $\mathbf{a}' \in V, \tilde{\varphi} \in H(0), \psi' \in H_e^1(0)$.

Remark. The Eqs. (C) and (C*) are equivalent and are both contained in (A) and (B) for $\omega > 0$. Hence the equation systems formed by

- (A), (B) and (C) or
- (A), (B) and (C*)

have not a unique solution for $\omega > 0$. Consequently the system of linear equations is singular and cannot be solved directly but iterative solvers work and may even converge faster.

Remark. Consider the system (A), (B) and (C*) for $\omega = 0$:

$$\begin{aligned}
&\left(\frac{1}{\mu}\,\mathbf{curl}\,\mathbf{a}, \mathbf{curl}\,\mathbf{a}'\right)_{\Omega_c} - \int_{\partial\Omega_c} \frac{1}{\mu}\,(\mathbf{curl}\,\mathbf{a}\times\mathbf{n})\cdot\mathbf{a}'\mathrm{d}S + \\
&\qquad\left(\sigma\,\mathbf{grad}\,(\tilde{\varphi}+\psi), \mathbf{a}'\right)_{\Omega_c} = 0 && \text{(2.46a)}\\
&-\left(\varepsilon\mathbf{a},\,\mathbf{grad}\,\tilde{\varphi}'\right)_{\Omega_c} + \int_{\partial\Omega_c}\varepsilon\mathbf{a}\cdot\mathbf{n}\,\tilde{\varphi}'\,\mathrm{d}S = 0 && \text{(2.46b)}\\
&-\left(\varepsilon\,\mathbf{grad}\,(\tilde{\varphi}+\psi),\,\mathbf{grad}\,\psi'\right)_{\Omega_a} + \int_{\partial\Omega_c}\varepsilon\psi'\,\mathbf{grad}\,\varphi\cdot\mathbf{n}\,\mathrm{d}S = 0. && \text{(2.46c)}
\end{aligned}$$

Eqs. (2.46a) and (2.46b) are the variational form of Eqs. (2.33b) and (2.33c). Eq. (2.46c) is the variational form of the Gauss Law (2.33a) outside the conductor and by setting $\mathbf{a}' = \mathbf{grad}\,\varphi$ in (2.46a) the Gauss Law inside the conductor Ω_w is recovered. Therefore the stationary Maxwell Equations (2.33) are contained in Eqs. (2.45) and robustness with respect to small values of ω (cf. [Hiptmair et al., 2008]) can be expected.

2.7 Impedance boundary conditions

Inside the IBC conductor the so called skin effect is observed: For high frequencies ω the electromagnetic fields decay exponentially in a thin boundary layer at the surface with penetration depth (cf. [Jackson, 1998, p. 220])

$$\delta := \sqrt{\frac{2}{\mu\sigma\omega}}.$$

According to [Ostrowski, 2002] δ is typically in the order of [0.05mm − 6.0mm] for steel. Hence a very high spatial resolution is needed to resolve this boundary layer correctly with a FE method which in turn leads to high computational costs. Instead the electromagnetic fields inside the IBC conductor are often not modeled at all and the impedance boundary conditions (IBC) (cf. [Ostrowski, 2002, p. 16])

$$\mathbf{n} \times \mathbf{e}_i = \eta_1 \cdot \mathbf{n} \times (\mathbf{n} \times \mathbf{h}_i), \tag{2.47}$$
$$\text{with } \eta_1 := (1+i)\sqrt{\frac{\mu_i\omega}{2\sigma_i}},$$

are used to approximate the fields on the surface of the conductor. Eq. (2.47) is derived (cf. [Jackson, 1998, p.355]) from Maxwell's Equations by assuming

- Zero displacement current in Ampere's Law (2.1d),
- The electrical field $\mathbf{e}$ outside of the conductor is perpendicular to the surface,
- The magnetic field strength $\mathbf{h}$ is parallel to the surface,
- Derivatives along the surface are small compared to derivatives in normal direction.

Because Eq. (2.47) is only valid inside the IBC conductor the subscript $_i$ was used to denote fields/variables which are measured inside the conductor.

With the help of the jump conditions [Nolting, 2007, p. 295]

$$[\mathbf{n} \times \mathbf{h}] = \mathbf{n} \times (\mathbf{h}_i - \mathbf{h}) = 0,$$
$$[\mathbf{n} \times \mathbf{e}] = \mathbf{n} \times (\mathbf{e}_i - \mathbf{e}) = 0.$$

the impedance boundary conditions on the outside are expressed as

$$\mathbf{n} \times \mathbf{e} = \eta_1 \cdot \mathbf{n} \times (\mathbf{n} \times \mathbf{h}), \tag{2.48}$$
$$\text{with } \eta_1 := (1+i)\sqrt{\frac{\mu_i\omega}{2\sigma_i}}. \tag{2.49}$$

Next $\mathbf{n}\times$ is applied to both sides of Eq. (2.48) and with the help of a vector identity an expression for $\mathbf{n} \times \mathbf{h}$ is obtained:

$$\begin{aligned}\mathbf{n} \times (\mathbf{n} \times \mathbf{e}) &= \eta_1 \cdot \mathbf{n} \times (\mathbf{n} \times (\mathbf{n} \times \mathbf{h})) \\ &= \eta_1 \cdot [(\mathbf{n} \cdot (\mathbf{n} \times \mathbf{h}))\mathbf{n} - \mathbf{n} \times \mathbf{h}] \\ &= -\eta_1 \cdot \mathbf{n} \times \mathbf{h}. \end{aligned} \tag{2.50}$$

Eq. (2.50) can also be stated in the $a - \varphi$ formalism:

$$\mathbf{n} \times (\mathbf{n} \times (\,\mathbf{grad}\,(\tilde{\varphi} + \psi) + i\omega\mathbf{a})) = \frac{\eta_1}{\mu} \cdot \mathbf{n} \times \mathbf{curl}\,\mathbf{a}.$$

Because $\psi = \text{const}$ on Γ_i it holds $(\mathbf{n} \times \,\mathbf{grad}\,\psi)|_{\Gamma_i} = 0$:

$$\mathbf{curl}\,\mathbf{a} \times \mathbf{n} = -\frac{\mu}{\eta_1} \cdot \mathbf{n} \times (\mathbf{n} \times (\,\mathbf{grad}\,\tilde{\varphi} + i\omega\mathbf{a})). \tag{2.51}$$

The above equation can now be substituted into the boundary term in Eq. (A).

2.8 Implemented variational equations

This section derives the variational formulation of a concrete problem with the boundary conditions (cf. [Hiptmair et al., 2008])

$$\begin{aligned} \mathbf{a} \times \mathbf{n} = 0, \qquad \varphi = lU \quad &\text{on } \Gamma_l,\ l = 0, 1,\ U \in \mathbb{C}, \\ \left.\begin{aligned} \mathbf{curl}\,\mu^{-1}\,\mathbf{curl}\,\mathbf{a} \cdot \mathbf{n} = 0 \\ \mathbf{curl}_\Gamma\,\mathbf{a_t} = 0, \quad \varepsilon\mathbf{a} \cdot \mathbf{n} = 0 \end{aligned}\right\} \ &\text{on } \Gamma_n, \\ \mathbf{curl}\,\mathbf{a} \times \mathbf{n} = -\frac{\mu}{\eta_1} \cdot \mathbf{n} \times (\mathbf{n} \times (\,\mathbf{grad}\,\tilde{\varphi} + i\omega\mathbf{a})) \quad &\text{on } \Gamma_i. \end{aligned}$$

Hiptmair et al. [2008] show that with this boundary conditions all boundary terms in the robust variational formulation on $\Gamma_n, \Gamma_0, \Gamma_1$ vanish. Therefore the variational formulation becomes:

$$\begin{aligned} &\left(\frac{1}{\mu}\,\mathbf{curl}\,\mathbf{a}, \mathbf{curl}\,\mathbf{a}'\right)_{\Omega_c} + \int_{\Gamma_i} \frac{1}{\eta_1} \cdot \mathbf{n} \times (\mathbf{n} \times (\,\mathbf{grad}\,\tilde{\varphi} + i\omega\mathbf{a})) \cdot \mathbf{a}'\,\mathrm{d}S - \\ &\quad \left((\omega^2\varepsilon - i\omega\sigma)\mathbf{a}, \mathbf{a}'\right)_{\Omega_c} + \left((i\omega\varepsilon + \sigma)\,\mathbf{grad}\,\tilde{\varphi}, \mathbf{a}'\right)_{\Omega_c} + \left(i\omega\varepsilon\,\mathbf{grad}\,\psi, \mathbf{a}'\right)_{\Omega_c} = 0 \end{aligned} \tag{A2}$$

$$-\left(\varepsilon\mathbf{a},\ \mathbf{grad}\,\tilde{\varphi}'\right)_{\Omega_c} + \int_{\Gamma_i} \varepsilon\mathbf{a} \cdot \mathbf{n}\,\tilde{\varphi}'\,\mathrm{d}S = 0 \tag{B2}$$

$$-\omega^2 \int_{\Gamma_i} \varepsilon\mathbf{a} \cdot \mathbf{n}\psi'\,\mathrm{d}S + \left(i\omega\varepsilon\,\mathbf{grad}\,(\tilde{\varphi} + \psi),\ \mathbf{grad}\,\psi'\right)_{\Omega_a} = 0 \tag{C2}$$

$$-\left(\varepsilon\,\mathbf{grad}\,(\tilde{\varphi} + \psi),\ \mathbf{grad}\,\psi'\right)_{\Omega_a} + \int_{\Gamma_i} \varepsilon\psi'\,\mathbf{grad}\,\varphi \cdot \mathbf{n}\,\mathrm{d}S = 0, \tag{C2*}$$

where we have used that

$$-\int_{\Gamma_i} \frac{1}{\mu}\,(\mathbf{curl}\,\mathbf{a} \times \mathbf{n}) \cdot \,\mathbf{grad}\,\psi'\,\mathrm{d}S = -\int_{\Gamma_i} \frac{1}{\mu}\,(\mathbf{n} \times \,\mathbf{grad}\,\psi') \cdot \mathbf{curl}\,\mathbf{a}\,\mathrm{d}S = 0,$$

because $\psi' \equiv \text{const}$ on Γ_i.

3 Implementation in HADAPT

This compact chapter explains the main features of the numerical discretization. It is assumed that the reader is familiar with the FE method and many technical details are left out.

3.1 Assembling the matrices

HADAPT uses a mesh composed of second order curved tetrahedrons to describe the geometry. Each tetrahedron is defined by 10 nodes (cf. Fig. 3.1) but only 4 locally linear, nodal shape functions exist per element. However the mapping from the reference element to the individual tetrahedron is second order and therefore the global shape functions will also be second order polynomials.

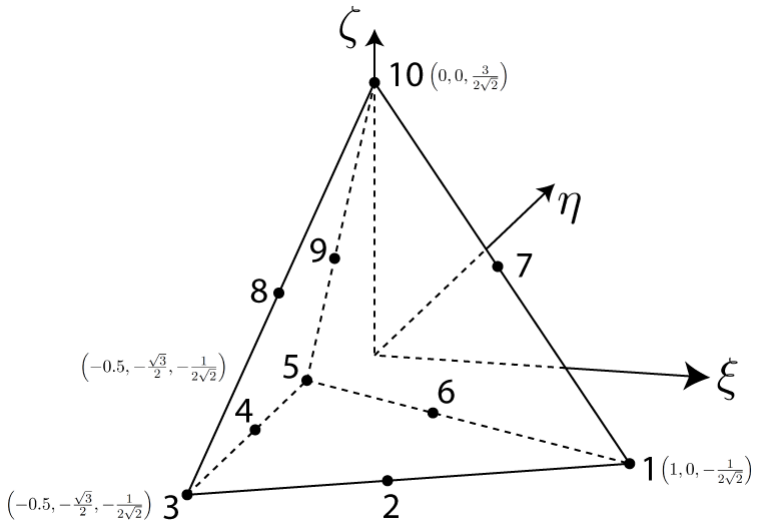

Figure 3.1: Reference Tetrahedron with node numbers and coordinates

For the vector potential **a** 6 vector valued edge basis functions are defined along the edges of the tetrahedron:

$$\varphi_A(\xi,\eta,\zeta)\,\mathbf{grad}\,\varphi_B(\xi,\eta,\zeta) - \varphi_B(\xi,\eta,\zeta)\,\mathbf{grad}\,\varphi_A(\xi,\eta,\zeta)$$

where φ_A, φ_B are the nodal basis functions of the two nodes which are connected by the edge. By convention node B is chosen to have the higher index.

The volume integrals appearing in the variational formulation (Eqs. (A2), (B2), (C2*)) are evaluated with a 4-point Gaussian quadrature rule whereas the boundary integration is calculated by a 7-point Gaussian quadrature rule (cf. [Greenough, 2000]).

3.2 Solving the equations

HADAPT provides two strategies to iteratively solve the resulting linear equations using BiCGStab. They only differ in the choice of the preconditioner:

The direct preconditioner first assembles a second system matrix with a σ-limiter, i.e. the entries are calculated by allowing a maximal conductivity of 10^5 [Sm^{-1}]. This leads to a system matrix which is then inverted with a direct LU decomposition to provide a preconditioner for the system to be solved.

BiCG Stab usually converges with this preconditioner in less than 15 steps to a solution with insignificant error. However due to the high memory requirements this preconditioner is only applicable to small systems.

The real valued preconditioner uses Operator preconditioning in conjunction with a Schur complement technique. Ostrowski et al. [2010] describe this technique in more detail.

This method enables the use of a larger number of unknowns and is often used in practice. Unfortunately it was not possible to implement the IBC with this preconditioner due to time constraints.

4 Numerical Experiments

In total three test cases are considered to test and verify the implementation of the IBC in HADAPT. Sec. 4.1 gives an accurate description of those test cases whereas Secs. 4.2 and 4.4 discuss the performance respectively the applicability of IBC. Sec. 4.3 compares the results to another commercial solver, Infolytica, which also supports IBC.

4.1 Description of test cases

1 Material test case This test case is very similar to the configuration described in Sec. 2.1: Voltage boundary conditions are placed on an (excitatory) conductor and cause a current which in turn induces currents in the IBC conductor (cf. Fig. 2.1 and Fig. 4.1) As the name suggests, impedance boundary conditions are used to approximate the surface currents of the IBC conductor.

The material properties are given in Tab. 4.1.

	$\sigma\,[\mathrm{Sm}^{-1}]$	ε_r	μ_r
Air box	0.	1.	1.
Excitatory conductor	$5e6$	1.	1.
IBC conductor	$1e7$	1.	200.

Table 4.1: Material Properties for 1 Material test case.
$\varepsilon = \varepsilon_0\varepsilon_r$, $\mu = \mu_0\mu_r$

2 Materials test case This problem is almost an exact duplicate of the 1 Material test case. The only difference is that the IBC conductor has been split into two IBC conductors with distinct material properties (cf. Fig. 4.2). The IBC are only used between the air box and the IBC conductors but not between the two IBC conductors.

The material properties are given in Tab. 4.2.

Short body test case In this problem we use the same setup as in the 1 Material test case but with an IBC conductor of half the length. The material properties are the same (cf. Tab. 4.1).

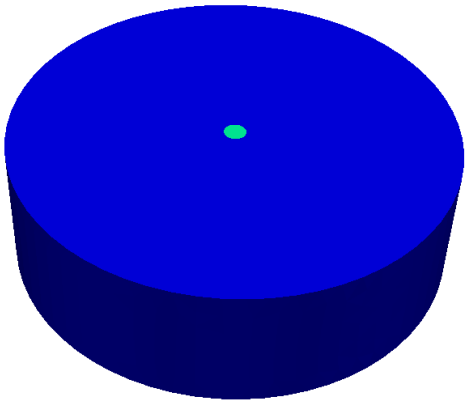

(a) With air box

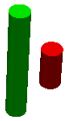

(b) Without air box

Figure 4.1: 1 Material test case. Blue = Air box, green = excitatory conductor, red = IBC conductor

	σ [Sm^{-1}]	ε_r	μ_r
Air box	0.	1.	1.
Excitatory conductor	$5e6$	1.	1.
IBC conductor A	$1e7$	1.	200.
IBC conductor B	$1e7$	1.	100.

Table 4.2: Material properties for 2 Material test case.

4.2 Runtime and memory requirements

The numerical experiments were performed on a 64-bit Intel Xeon Quad core with 8Gb RAM. The termination criteria for BiCGStab was set to $1.0 \cdot 10^{-10}$.

The total runtimes to solve each of the three configurations (see Sec. 4.1) with IBC and by fully resolving the boundary layer are shown in Fig. 4.4. In Fig. 4.5 the memory requirements along with the degrees of freedom (dof) of the resulting linear system are plotted for each configuration.

It is observed that the IBC generally lead to a decrease in the dof of each configuration because the interior of the IBC conductor(s) is not modeled. Because many dofs are needed to properly resolve the boundary layers IBC really reduce the number of unknowns which in turn results in shorter run times and less memory consumption. For the configurations under consideration simulation time and memory consumption was

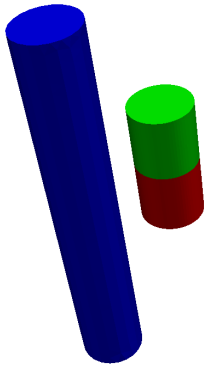

Figure 4.2: 2 Materials test case without air box. Blue = Excitatory conductor, Green = IBC Conductor A, Red = IBC Conductor B.

reduced by $25\% - 45\%$ by using IBC as opposed to a fully resolved model.

4.3 Comparison to Infolytica

In order to verify the implementation of the IBC the first two test cases described in Sec. 4.1 were also calculated with Infolytica. Infolytica doesn't use the stabilized formulation and smoothes the resulting fields to get a better visualization but it also supports IBC.

Fig. 4.6 and Fig. 4.7 show the root mean squared (RMS) surface $\mathbf{j}$ and $\mathbf{b}$ field, respectively. Qualitatively both fields look very similar and the upper and the lower value appear to be almost exactly the same. This proves that the IBC implementation in HADAPT is indeed giving correct results.

Potential of IBC conductor The Stabilized Maxwell Formulation is able to determine the potential on the IBC conductor which is not possible with the usual formulation that is used e.g. by Infolytica. Fig. 4.8 shows this for the 1 material configuration. It is seen that the potential of the IBC conductor forms one equipotential surface that has the value 0.5. This is exactly what is observed in an experiment.

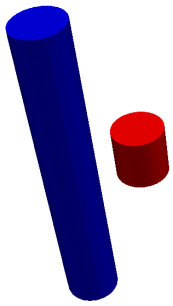

Figure 4.3: Short body test case without air box. Blue = Excitatory conductor, Red = IBC Conductor.

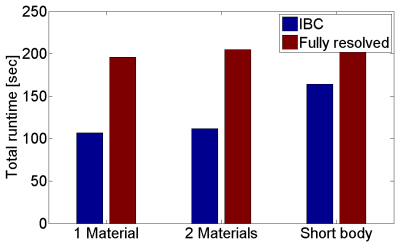

Figure 4.4: Total runtime for different configurations.

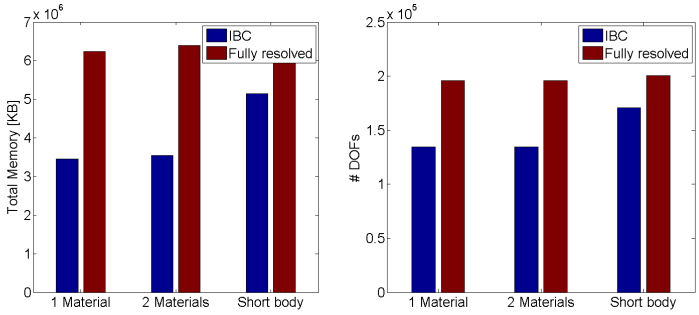

Figure 4.5: Memory consumption and degrees of freedom for different configurations

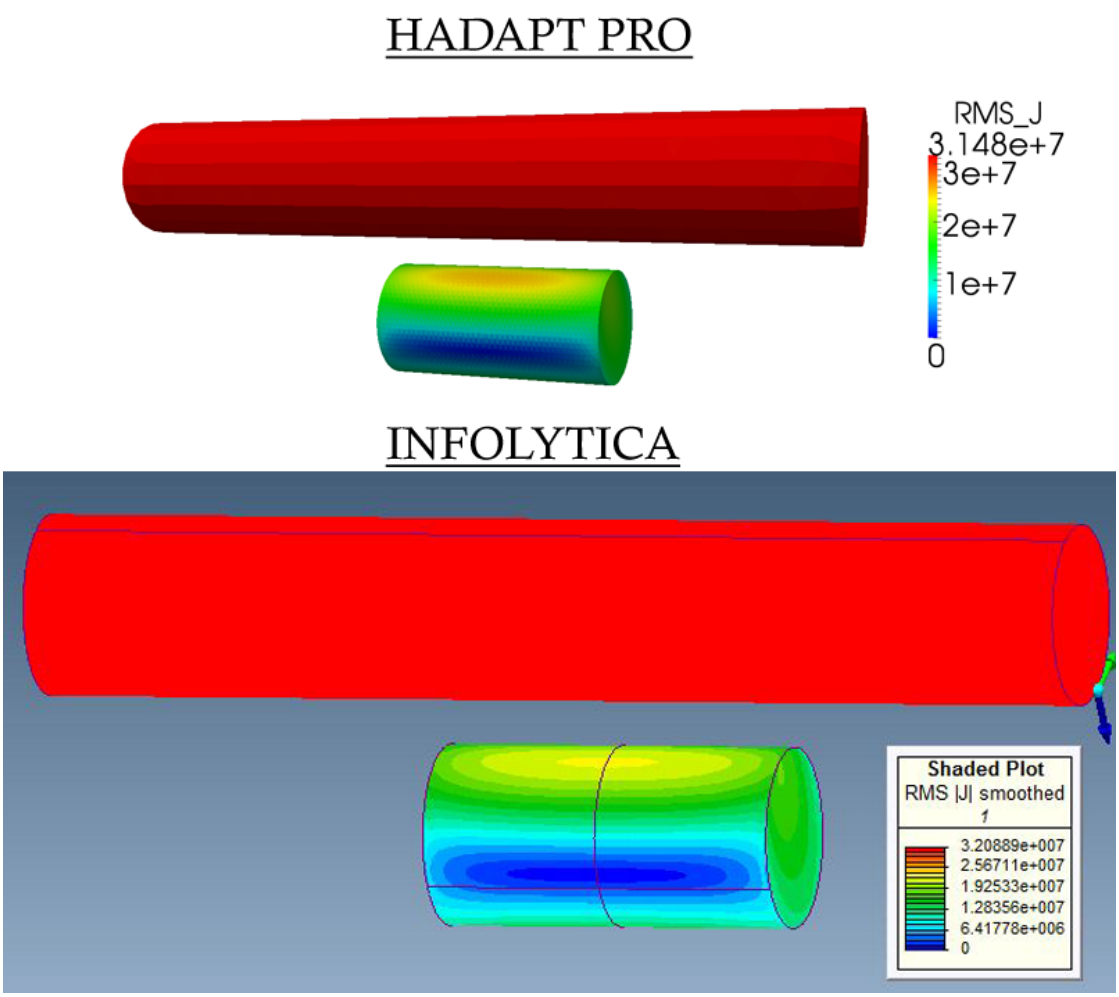

Figure 4.6: The surface current in [A] calculated with HADAPT and Infolytica for 1 material test case.

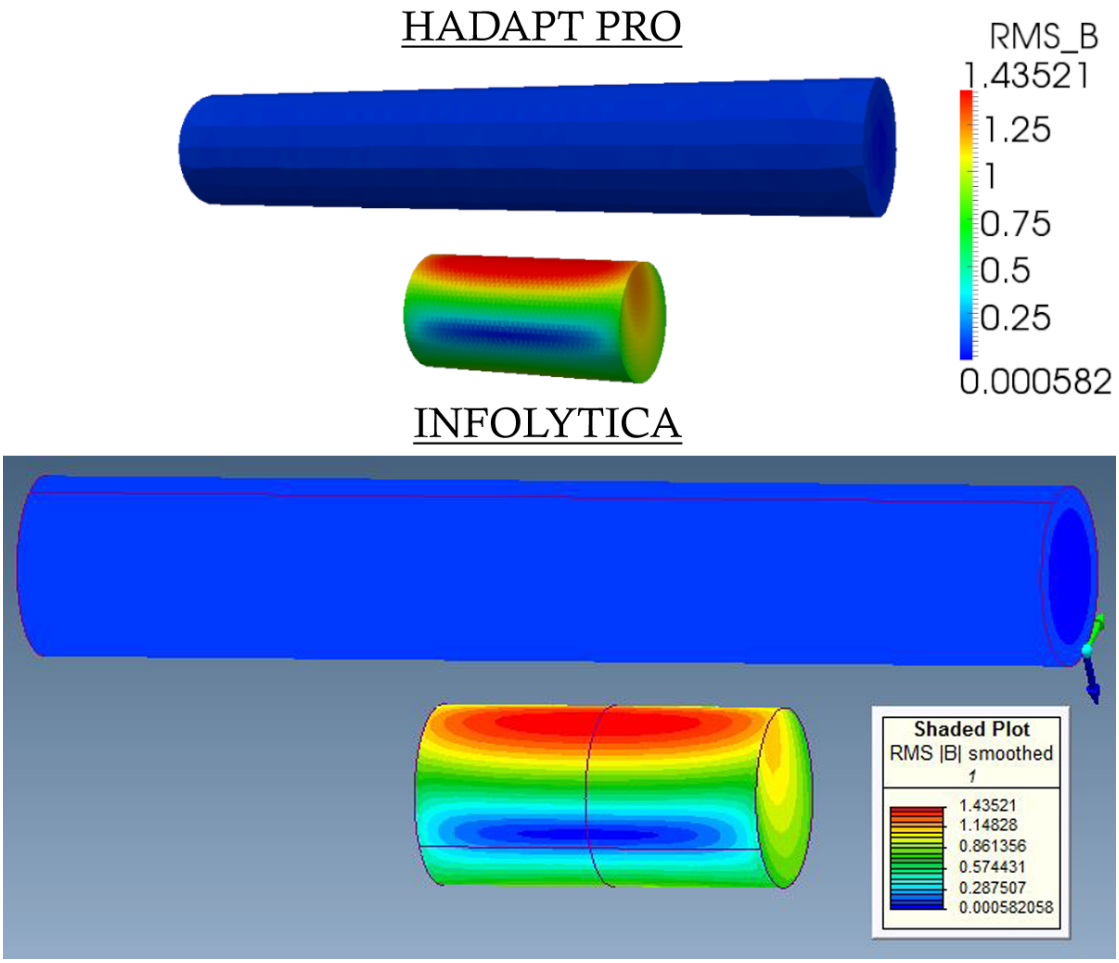

Figure 4.7: The surface B-field in [T] calculated with HADAPT and Infolytica for 1 material configuration.

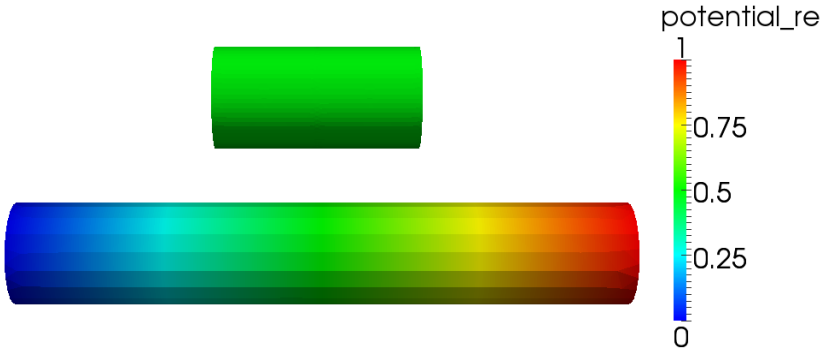

Figure 4.8: Real part of the potential φ in [V] for the 1 Material test case.

4.4 Accuracy of the IBC

The better performance of IBC is bought by a strong approximation: the interior of the IBC conductor is approximated by a surface model. In order to measure the approximation error the IBC solution is compared to the fully resolved model by computing the *relative* L^2 and L^∞ norms,

$$\|\varphi_{\text{IBC}} - \varphi_{\text{full}}\|_{\text{relative}} = \frac{\|\varphi_{\text{IBC}} - \varphi_{\text{full}}\|}{\|\varphi_{\text{full}}\|}.$$

All norms are calculated over the computational domain Ω_c.

Fig. 4.9 shows the L^2 and L^∞ norms for the computational variables φ and A at 50Hz. For φ the relative L^2 norm is in the range of $0.4\% - 0.6\%$ and for A in the order of $1\% - 1.5\%$. The L^∞ norm is higher for all test cases and lies in between $0.13\% - 0.14\%$ and $2.5\% - 3\%$, respectively. The results show that IBC indeed approximate the physical solution closely.

One would expect a higher norm for the short body test than for the other configurations because the third assumption of the IBC (see Sec. 2.7) is more violated. But Fig. 4.9 shows that the difference to the fully resolved model is almost independent of the chosen configuration. Further investigations with more complex geometries are needed to better judge the applicability of IBC for a given configuration.

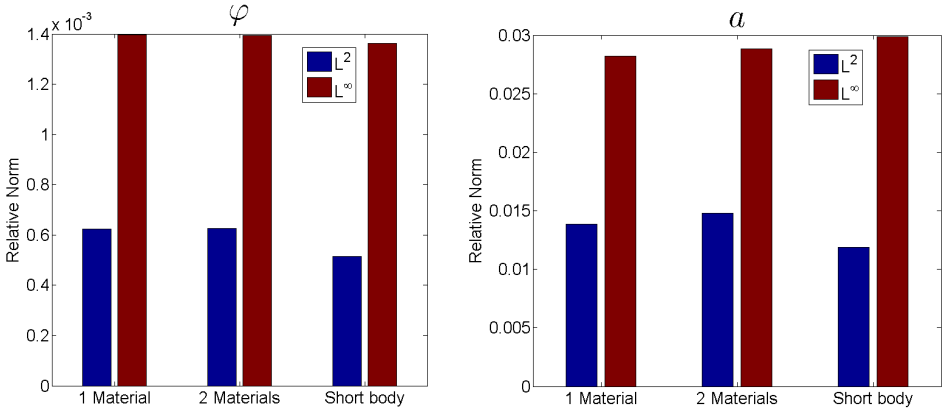

Figure 4.9: Relative norms of the difference between full and IBC solution at 50Hz.

Fig. 4.10 shows the relative norms for different frequencies. While the relative norm of the potential φ increases linearly with higher frequencies, the norm of the vector potential $\mathbf{a}$ decreases in a nonlinear fashion. This could result from the fully resolved model not being able to completely resolve the boundary layer because its thickness decreases with higher frequency. Therefore studies with more accurate, fully resolved models are needed to better understand this effect.

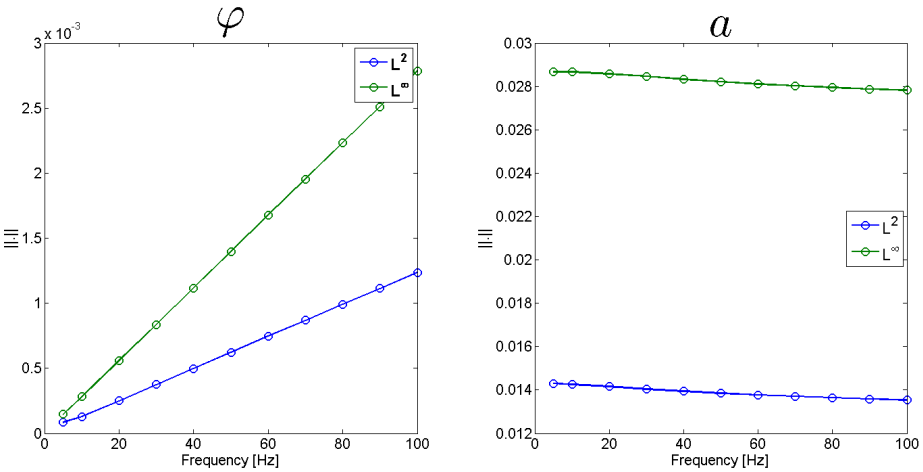

Figure 4.10: Dependence of the relative norms on the frequency for 1 material test case.

5 Conclusion

In this study IBC were successfully implemented in HADAPT and tested thoroughly. They provide an efficient way to resolve boundary layers in conductors by reducing the degrees of freedom. Generally IBC are advantageous to a fully resolved model at high frequencies because the boundary layer becomes narrower with increasing frequency and with it the DOF's needed to resolve the boundary layer.

Usually IBC are implemented based on the standard Maxwell's equations and the electric potential of the IBC conductor cannot be calculated in a stable way. This study showed that the introduction of an extra unknown (cf. Hiptmair et al. [2008]) allows for a robust calculation of this potential.

It was also shown that for geometrically simple test geometries the runtime and memory requirements were reduced substantially while keeping the total error at a few percents. While the approximation error clearly depends on the frequency, it is almost independent of the geometry which has to be confirmed for more complex, real-world configurations.

The present implementation only allows the direct preconditioner to be used with IBC. In order to simulate more complex geometries with vastly more unknowns the code has to be extended to work with the real valued preconditioner as well.

Bibliography

Chris Greenough. *The Finite Element Library (Release 4.0) - Level 0 User Documentation*. Rutherford Appleton Laboratory, December 2000. URL `http://www.softeng.rl.ac.uk/st/projects/felib4/Docs/PDF/Level-0.pdf`. (Cited on page 15.)

Ralf Hiptmair, Florian Kramer, and Joerg Ostrowski. A robust maxwell formulation for all frequencies. *Magnetics, IEEE Transactions on*, 44(6):682 –685, june 2008. (Cited on pages c, 2, 3, 7, 9, 11, 13 and 24.)

John David Jackson. *Classical Electrodynamics*. Wiley, third edition, 1998. ISBN 978-0471309321. (Cited on pages 1 and 12.)

Wolfgang Nolting. *Grundkurs Theoretische Physik*, volume 3: Elektrodynamik. Springer-Verlag, eight edition, 2007. ISBN 978-3-540-71251-0. (Cited on pages 4, 5 and 12.)

Jörg Ostrowski. *Boundary element methods for inductive hardening*. PhD thesis, Universität Tübingen, 2002. URL `http://tobias-lib.uni-tuebingen.de/volltexte/2003/672`. (Cited on page 12.)

Jörg Ostrowski, Mario Bebendorf, Ralf Hiptmair, and Florian Krämer. $\mathcal{H}$-matrix-based operator preconditioning for full Maxwell at low frequencies. *IEEE Trans. Magn.*, 46 (8), 2010. (Cited on page 15.)